Eur. Phys. J. A **21**, 117–131 (2004)
DOI 10.1140/epja/i2003-10179-x

THE EUROPEAN PHYSICAL JOURNAL A

Chiral approach to nuclear matter: Role of explicit short-range NN-terms

S. Fritsch[1,2] and N. Kaiser[1,a]

[1] Physik Department T39, Technische Universität München, D-85747 Garching, Germany
[2] ECT*, I-38050 Villazzano (Trento), Italy

Received: 28 October 2003 / Revised version: 9 December 2003 /
Published online: 23 July 2004 –
Communicated by U.-G. Meißner

Abstract. We extend a recent chiral approach to nuclear matter by including the most general (momentum-independent) *NN*-contact interaction. Iterating this two-parameter contact vertex with itself and with one-pion exchange the emerging energy per particle exhausts all terms possible up to and including fourth order in the small momentum expansion. Two (isospin-dependent) cut-offs $\Lambda_{0,1}$ are introduced to regularize the (linear) divergences of some three-loop in-medium diagrams. The equation of state of pure neutron matter, $\bar{E}_n(k_n)$, can be reproduced very well up to quite high neutron densities of $\rho_n = 0.5\,\mathrm{fm}^{-3}$ by adjusting the strength of a repulsive nn-contact interaction. Binding and saturation of isospin-symmetric nuclear matter is a generic feature of our perturbative calculation. Fixing the maximum binding energy per particle to $-\bar{E}(k_{f0}) = 15.3\,\mathrm{MeV}$ we find that any possible equilibrium density ρ_0 lies below $\rho_0^{\max} = 0.191\,\mathrm{fm}^{-3}$. The additional constraint from the neutron matter equation of state leads however to a somewhat too low saturation density of $\rho_0 = 0.134\,\mathrm{fm}^{-3}$. We also investigate the effects of the *NN*-contact interaction on the complex single-particle potential $U(p,k_f) + i\,W(p,k_f)$. We find that the effective nucleon mass at the Fermi surface is bounded from below by $M^*(k_{f0}) \geq 1.4M$. This property keeps the critical temperature of the liquid-gas phase transition at somewhat too high values $T_c \geq 21\,\mathrm{MeV}$. The downward bending of the asymmetry energy $A(k_f)$ above nuclear-matter saturation density is a generic feature of the approximation to fourth order. We furthermore investigate the effects of the *NN*-contact interaction on the $(\vec{\nabla}\rho)^2$-term in the nuclear energy density functional $\mathcal{E}[\rho,\tau]$. Altogether, there is within this complete fourth-order calculation no "magic" set of adjustable short-range parameters with which one could reproduce simultaneously and accurately all semi-empirical properties of nuclear matter. In particular, the conditions for a good neutron matter equation of state and for good single-particle properties are mutually exclusive.

PACS. 12.38.Bx Perturbative calculations – 21.65.+f Nuclear matter – 24.10.Cn Many-body theory – 31.15.Ew Density-functional theory

1 Introduction

The present status of the nuclear-matter problem is that a quantitatively successful description can be achieved, using advanced many-body techniques, in a non-relativistic framework when invoking an adjustable three-nucleon force [1]. Alternative relativistic mean-field approaches, including either non-linear terms with adjustable parameters or explicitly density-dependent point couplings, are also widely used for the calculation of nuclear-matter properties and of finite nuclei [2–5]. At a more basic level, the Dirac-Brueckner method of ref. [6] solves a relativistically improved Bethe-Goldstone equation with one-boson exchange *NN*-interactions.

In recent years a novel approach to the nuclear-matter problem based on effective field theory (in particular chiral perturbation theory) has emerged [7–9]. The key element there is a separation of long- and short-distance dynamics and an ordering scheme in powers of small momenta. At nuclear-matter saturation density the Fermi momentum k_{f0} and the pion mass m_π are comparable scales ($k_{f0} \simeq 2m_\pi$), and therefore pions must be included as explicit degrees of freedom in the description of the nuclear many-body dynamics. The contributions to the energy per particle $\bar{E}(k_f)$ of isospin-symmetric nuclear matter as they originate from chiral pion-nucleon dynamics have been computed up to three-loop order in refs. [7,8]. Both calculations include the 1π-exchange Fock diagram and the iterated 1π-exchange Hartree and Fock diagrams. In ref. [8] irreducible 2π-exchange has also been taken into account

[a] e-mail: nkaiser@ph.tum.de

and a momentum cut-off Λ has been used to regularize the few divergent parts associated with chiral 2π-exchange. The resulting cut-off–dependent contribution ($\bar{E}(k_f) \sim \Lambda k_f^3$, see eq. (15) in ref. [8]) is completely equivalent to that of a zero-range *NN*-contact interaction. At that point the (earlier) work by Lutz *et al.* [7] follows a different strategy. Two zero-range *NN*-contact interactions (acting in the $^3S_1$ and $^1S_0$ *NN*-states) proportional to the dimensionless parameters $g_0 + g_A^2/4$ and $g_1 + g_A^2/4$ are explicitly introduced (see eq. (4) in ref. [7]). The components proportional to $g_A^2/4$ cancel (order by order) the zero-range contributions generated by one-pion exchange. The other components proportional to g_0 and g_1 are understood to subsume all non-perturbative short-range *NN*-dynamics relevant at densities around nuclear-matter saturation density ρ_0.

Despite their differences in the treatment of the effective short-range *NN*-dynamics both chiral approaches [7,8] are able to reproduce correctly several empirical nuclear-matter properties (saturation density ρ_0, binding energy per particle $-\bar{E}(k_{f0})$ and compressibility $K = k_{f0}^2 \bar{E}''(k_{f0})$) by fine-tuning only one parameter, either the coupling $g_0 + g_1 \simeq 3.23$ or the cut-off $\Lambda \simeq 0.65\,\mathrm{GeV}$. The fine-tuning of a momentum cut-off Λ as done in ref. [8] introduces some degree of non-uniqueness that lies outside chiral perturbation theory. One should, however, keep in mind that fine-tuning of some parameter(s) is involved in most calculations of nuclear matter.

Although the conceptual treatment of the short-range *NN*-interaction by Lutz *et al.* [7] may be very appealing at first sight, it suffers (after a closer inspection) from severe phenomenological problems. As shown recently in ref. [10] the single-particle properties come out completely unrealistic in this scheme. The potential depth of $U(0, k_{f0}) = -20\,\mathrm{MeV}$ is by far too weakly attractive, while, on the other hand, the imaginary single-particle potential $W(0, k_{f0}) = 51\,\mathrm{MeV}$ is too large. Most seriously, the total single-particle energy $T_{\mathrm{kin}}(p) + U(p, k_{f0})$ does not rise monotonically with the nucleon momentum p, thus implying a negative effective nucleon mass at the Fermi surface $p = k_{f0}$ (see fig. 3 in ref. [10]). In such an abnormal situation there exist occupied nucleon states in the Fermi sea with total energy higher than the Fermi energy, indicating an instability of the system. As a matter of fact the overly strong momentum dependence of the nuclear mean-field $U(p, k_f)$ in the scheme of Lutz *et al.* [7] (leading to $\partial U/\partial p < -p/M$) originates from those diagrams in which the (strong and) attractive *NN*-contact interaction (proportional to $g_0 + g_1 + g_A^2/2$) is further iterated. The *NN*-contact interaction necessarily has to be very strong in this scheme since it effectively also has to account for the attraction generated dynamically by iterated 1π-exchange in form of a (regularization-dependent) linear divergence $\int_0^\infty \mathrm{d}l\, 1$. In contrast to that much better single-particle properties have been obtained in the chiral approach of ref. [9] employing cut-off regularization and not introducing any explicit short-range *NN*-terms. For example, the resulting potential depth of $U(0, k_{f0}) = -53\,\mathrm{MeV}$ [9] is in good agreement with the depth of the empirical nuclear shell model potential [11] or the optical model potential [12]. Furthermore, when extended to finite temperatures this approach reproduces the first-order liquid-gas phase transition of isospin-symmetric nuclear matter, however, with a somewhat too high value of the critical temperature $T_c = 25\,\mathrm{MeV}$ [13]. The reason for that is a still too strong momentum dependence of the real single-particle potential $U(p, k_{f0})$ near the Fermi surface $p = k_{f0}$ [9].

The purpose of the present paper is to investigate in detail the role of short-range *NN*-terms in addition to pion-exchange dynamics for a variety of nuclear-matter observables. Our primary interest is to find out whether such adjustable *NN*-contact terms (of moderate strength) can cure certain shortcomings of previous calculations [8, 9] which have included only the pion-exchange contributions to three-loop order. From the point of view of the expansion in powers of small momenta (k_f and m_π) the combination of pion-exchange and zero-range *NN*-contact interaction exhausts actually all terms possible up to and including fourth order. Alternatively, the interacting part of the energy per particle can be understood (within this approximation to order $\mathcal{O}(k_f^4)$) as to result from the Hartree and Fock contributions of a nucleon-nucleon T-matrix of the form:

$$\mathcal{T}_{NN} = \frac{g_A^2}{4f_\pi^2}\left[\frac{\vec{\sigma}_1\cdot\vec{q}\;\vec{\sigma}_2\cdot\vec{q}}{m_\pi^2+\vec{q}^{\,2}}\,\vec{\tau}_1\cdot\vec{\tau}_2 + \frac{\gamma_0+3\gamma_1}{2} + \frac{\gamma_1-\gamma_0}{2}\,\vec{\tau}_1\cdot\vec{\tau}_2\right], \tag{1}$$

which is evaluated in first- and second-order perturbation theory (*i.e.* it is also iterated once with itself). Note that additional spin-spin terms proportional to $\vec{\sigma}_1\cdot\vec{\sigma}_2$ are redundant in the T-matrix eq. (1) as a consequence of the Pauli exclusion principle. The two coefficients, γ_0 and γ_1, parameterize the strength of the contact interaction in *NN*-states with total isospin $I = 0, 1$. In order to have immediately a measure of the (relative) magnitudes involved we note that the repulsive contact piece which survives from one-pion exchange in the chiral limit $m_\pi = 0$ can be mapped onto $\gamma_0^{(1\pi)} = \gamma_1^{(1\pi)} = -1/2$. As usual, $f_\pi = 92.4\,\mathrm{MeV}$ denotes the pion decay constant and $m_\pi = 135\,\mathrm{MeV}$ stands for the (neutral) pion mass. The value $g_A = 1.3$ of the nucleon axial-vector coupling constant is linked via the Goldberger-Treiman relation to a πNN-coupling constant of $g_{\pi N} = g_A M/f_\pi = 13.2$ [14]. The iteration of the T-matrix eq. (1) to second order generates besides finite terms also the (primitive) linearly divergent loop-integral $\int_0^\infty \mathrm{d}l\, 1$. As done in ref. [8] it will be regularized by a momentum cut-off $\Lambda_{0,1}$ which we allow in this work to depend on the total isospin $I = 0, 1$ of the two-nucleon system[1]. Such a doubling procedure is physically meaningful since cut-off–dependent contributions are fully equivalent to contributions from (momentum-independent) *NN*-contact vertices. On the practical side

[1] The weighting factors of Λ_0 and Λ_1 are readily found by decomposing the isospin factor of a particular diagram into the projection operators on total isospin $I = 0, 1$: $\mathcal{P}_0 = (1 - \vec{\tau}_1\cdot\vec{\tau}_2)/4$ and $\mathcal{P}_1 = (3 + \vec{\tau}_1\cdot\vec{\tau}_2)/4$.

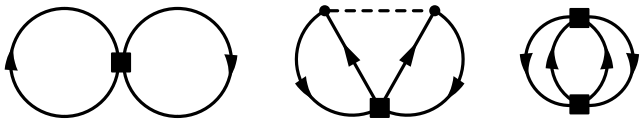

Fig. 1. Additional in-medium diagrams generated by the NN-contact interaction. The filled square vertex symbolizes this zero-range NN-contact interaction proportional to γ_0 and γ_1. The indices $I = 0, 1$ label the total isospin of the NN system.

four free parameters, $\gamma_{0,1}$ and $\Lambda_{0,1}$ give us more flexibility in adjusting nuclear-matter properties (within the present perturbative scheme). Of course, the two cut-offs $\Lambda_{0,1}$ should not differ too much from each other and they should also take on physically reasonable values.

2 Neutron matter equation of state

We start the discussion with the equation of state of pure neutron matter. For this system the total isospin of two nucleons is restricted to $I = 1$ and therefore only the strength parameter γ_1 (see eq. (1)) and the isospin-1 cut-off Λ_1 can come into play. We first write down the contributions to the energy per neutron $\bar{E}_n(k_n)$ generated by the zero-range nn-contact interaction proportional to γ_1. The left diagram in fig. 1 obviously leads to a contribution linear in the neutron density $\rho_n = k_n^3/3\pi^2$. Of the same structure are all the cut-off–dependent terms from iterated diagrams with two medium insertions[2]. We combine them by introducing the dimensionless parameter Γ_1:

$$\bar{E}_n(k_n) = -\frac{\Gamma_1 g_A^2 k_n^3}{6(2\pi f_\pi)^2}\,,$$

$$\Gamma_1 = \gamma_1 + \frac{g_A^2 M \Lambda_1}{(4\pi f_\pi)^2}(2\gamma_1 - 1)^2\,. \qquad (2)$$

The second diagram in fig. 1 with two medium insertions on parallel nucleon lines gives rise to a finite (*i.e.* cut-off–independent) contribution of the form

$$\bar{E}_n(k_n) = \frac{\gamma_1 g_A^4 M m_\pi^4}{5(8\pi)^3 f_\pi^4}\Big[22u - \frac{1}{u} - 4(5+4u^2)\arctan 2u + \Big(\frac{1}{4u^3} + \frac{5}{u}\Big)\ln(1+4u^2)\Big]\,, \qquad (3)$$

with $u = k_n/m_\pi$ the ratio of the neutron Fermi momentum k_n and the pion mass m_π. These two quantities are treated as small momentum/mass scales in our perturbative calculation. The second and third diagram in fig. 1 with three medium insertions represent Pauli-blocking effects. The corresponding contribution to the energy per neutron reads

$$\begin{aligned}\bar{E}_n(k_n) = {}& \frac{3\gamma_1 g_A^4 M m_\pi^4}{(4\pi f_\pi)^4 u^3}\int_0^u \mathrm{d}x\, x^2 \int_{-1}^1 \mathrm{d}y\,\Big[2uxy \\ & + (u^2 - x^2y^2)H\Big]\Big[(\gamma_1 - 1)s^2 + \ln(1+s^2)\Big] = \\ & \gamma_1 M\Big(\frac{g_A m_\pi}{4\pi f_\pi}\Big)^4\Big\{(\gamma_1 - 1)\frac{8u^4}{35}(11 - 2\ln 2) \\ & + \frac{8u^2}{5}(3 - \ln 2) - \frac{1}{2} - 4u\arctan 2u + \Big(\frac{3}{2} + \frac{1}{8u^2}\Big) \\ & \times \ln(1+4u^2) + \frac{3}{2u^3}\int_0^u \mathrm{d}x(u^2 - x^2)\Big[(1 + u^2 - x^2) \\ & \times \ln\frac{1+(u+x)^2}{1+(u-x)^2} + 4x\Big[\arctan 2x - \arctan(u+x) \\ & - \arctan(u-x)\Big] - \ln(1+4x^2)\Big]\ln\frac{u+x}{u-x}\Big\}\,, \qquad (4)\end{aligned}$$

with the auxiliary functions $H = \ln(u + xy) - \ln(u - xy)$ and $s = xy + \sqrt{u^2 - x^2 + x^2y^2}$. The quantity s has the geometrical meaning of the distance between a point on a sphere of radius u and an interior point displaced at a distance x from the center of the sphere. In the same geometrical picture y denotes a directional cosine. Note that iterated three-loop diagrams carry an energy denominator equal to the difference of nucleon kinetic energies and therefore they are proportional to the (large) nucleon mass $M = 939\,\mathrm{MeV}$. The additional contributions to $\bar{E}_n(k_n)$ from the (relativistically improved) kinetic energy, from 1π-exchange and from iterated 1π-exchange have been written down in eqs. (32)-(37) of ref. [8]. In the case of the 1π-exchange contribution (see eq. (33) in ref. [8]) we neglect of course the small relativistic $1/M^2$-correction of order $\mathcal{O}(k_f^5)$. Note that the parameter Γ_1 defined in eq. (2) includes also the cut-off–dependent contribution from iterated 1π-exchange (see eq. (39) in ref. [8]) through its γ_1-independent piece.

The full line in fig. 2 shows the energy per particle $\bar{E}_n(k_n)$ of pure neutron matter as a function of the neutron density $\rho_n = k_n^3/3\pi^2$. The dashed line stems from the many-body calculation of the Urbana group [1]. This line should be considered as a representative of the host of realistic neutron matter calculations [15,16] which scatter around it. The full line in fig. 2 has been obtained by adjusting the parameter γ_1 to the value $\gamma_1 = -0.75$. This number translates into a repulsive zero-range nn-contact interaction which is comparable in strength to the 1π-exchange. (Remember that the contact piece of 1π-exchange maps onto $\gamma_1^{(1\pi)} = -1/2$). The other parameter Γ_1 regulating an attractive contribution to $\bar{E}_n(k_n)$ linear in the neutron density ρ_n takes the value $\Gamma_1 = 2.76$. The cut-off scale $\Lambda_1 \simeq 0.48\,\mathrm{GeV}$ which parameterizes (via the relation in eq. (2)) this amount of attraction linear in density lies well within the physically reasonable range. One observes that the result of the realistic neutron matter calculation of ref. [1] can be reproduced up to quite high neutron densities $\rho_n \leq 0.5\ \mathrm{fm}^{-3}$. In particular, the downward bending of $\bar{E}_n(k_n)$ above $\rho_n \geq 0.2\,\mathrm{fm}^{-3}$ which showed up

[2] This is a technical notation for the difference between the in-medium and vacuum nucleon propagator. For further details, see sect. 2 in ref. [8].

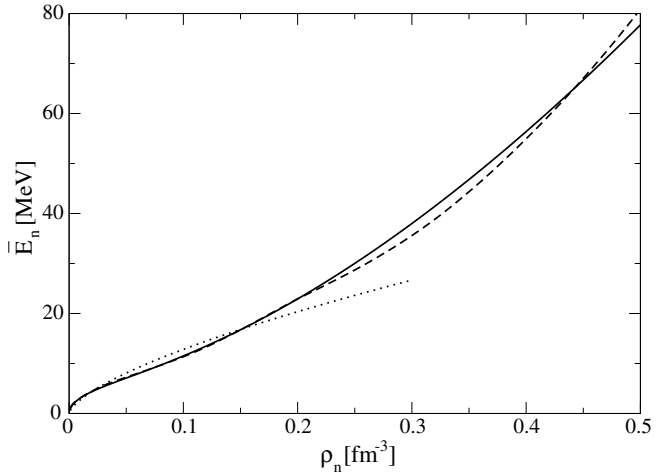

Fig. 2. The energy per particle $\bar{E}_n(k_n)$ of pure neutron matter *versus* the neutron density $\rho_n = k_n^3/3\pi^2$. The full line is obtained by adjusting the strength parameter of the *nn*-contact interaction to $\gamma_1 = -0.75$ together with a cut-off $\Lambda_1 = 0.48\,\mathrm{GeV}$. The dashed line stems from the many-body calculation of the Urbana group [1]. The dotted line gives one half of the kinetic energy $\bar{E}_{\rm kin}(k_n)/2 = 3k_n^2/20M$.

in fig. 8 of ref. [8] (including only pion-exchanges) is now eliminated. Note that in the scheme of Lutz *et al.* [7] this downward bending also persisted (see fig. 6 in ref. [10]). Altogether, it seems that most of the dynamics underlying the neutron matter equation of state (at moderate densities $\rho_n \leq 0.5\,\mathrm{fm}^{-3}$) can be covered by pion-exchange and a comparably strong short-distance *nn*-repulsion treated up to three-loop order. At low densities, $\rho_n < 0.2\,\mathrm{fm}^{-3}$, the equation of state of pure neutron matter is surprisingly well approximated by just one half of the kinetic energy, $\bar{E}_{\rm kin}(k_n)/2 = 3k_n^2/20M$, (see the dotted line in fig. 2) as emphasized recently in ref. [17].

3 Equation of state of isospin-symmetric nuclear matter

In this section we turn to the equation of state of isospin-symmetric nuclear matter. In this system with proton-to-neutron ratio equal to one both total *NN*-isospins $I = 0, 1$ are present and therefore all four parameters $\gamma_{0,1}$ and $\Lambda_{0,1}$ come into play. Following the scheme in sect. 2 we first enumerate the contributions to the energy per particle $\bar{E}(k_f)$ generated by the zero-range *NN*-contact vertex. The complete term linear in the nucleon density $\rho = 2k_f^3/3\pi^2$ can again be compactly written by introducing a new parameter $\mathit{\Gamma}_0$ which subsumes cut-off–dependent pieces in the $I = 0$ channel:

$$\bar{E}(k_f) = -\frac{(\mathit{\Gamma}_0 + \mathit{\Gamma}_1) g_A^2 k_f^3}{(4\pi f_\pi)^2}\,,$$
$$\mathit{\Gamma}_0 = \gamma_0 + \frac{g_A^2 M \Lambda_0}{(4\pi f_\pi)^2}(4\gamma_0^2 - 4\gamma_0 + 9)\,. \qquad (5)$$

The second pion-exchange diagram in fig. 1 with two medium insertions on parallel nucleon lines leads to the following finite (*i.e.* cut-off–independent) contribution:

$$\bar{E}(k_f) = \frac{3(\gamma_0+\gamma_1) g_A^4 M m_\pi^4}{10(8\pi)^3 f_\pi^4}\Big[22u - \frac{1}{u} - 4(5+4u^2) \times \arctan 2u + \left(\frac{1}{4u^3} + \frac{5}{u}\right)\ln(1+4u^2)\Big]\,, \qquad (6)$$

where the meaning of u has changed in this and all following sections to $u = k_f/m_\pi$. Diagrams with three medium insertions represent Pauli-blocking effects in isospin-symmetric nuclear matter. Their contribution to the energy per particle reads

$$\bar{E}(k_f) = \frac{9 g_A^4 M m_\pi^4}{2(4\pi f_\pi)^4 u^3} \times \int_0^u \mathrm{d}x\, x^2 \int_{-1}^1 \mathrm{d}y \Big[2uxy + (u^2 - x^2y^2)H\Big] \times \Big[(\gamma_0^2+\gamma_1^2-\gamma_0-\gamma_1)s^2 + (\gamma_0+\gamma_1)\ln(1+s^2)\Big]\,, \qquad (7)$$

where the linear/quadratic term in $\gamma_{0,1}$ obviously belongs the second/third diagram in fig. 1. For further reduction of the occurring double integral, see eq. (4). The expansion of the energy per particle up to order $\mathcal{O}(k_f^4)$ is completed by adding to the terms eqs. (5)-(7) the contribution from the (relativistically improved) kinetic energy, (static) 1π-exchange and iterated 1π-exchange written down in eqs. (5)-(11) of ref. [8].

Let us first look at generic properties of the nuclear-matter equation of state in our calculation. Binding and saturation occurs in a wide range of the three relevant combinations of parameters: $\mathit{\Gamma}_0 + \mathit{\Gamma}_1$, $\gamma_0 + \gamma_1$ and $\gamma_0^2 + \gamma_1^2$. We fix the negative minimum of the saturation curve $\bar{E}(k_f)$ to the value $-15.3\,\mathrm{MeV}$ [18] by adjusting at given (γ_0, γ_1) the strength $\mathit{\Gamma}_0 + \mathit{\Gamma}_1$ of the term linear in the density ρ appropriately. The horizontal position of each minimum determines then the corresponding saturation density $\rho_0(\gamma_0, \gamma_1) = \rho_0(\gamma_1, \gamma_0)$. It is obviously symmetric under the exchange of the two parameters $\gamma_0 \leftrightarrow \gamma_1$. In fig. 3, we show contours of constant saturation density ρ_0 in the (γ_0, γ_1)-plane. To a good approximation these contours are concentric circles around a point in parameter space where the saturation density becomes maximal. We find numerically the following approximate parameter dependence of the saturation density (in units of fm^{-3}):

$$\rho_0[\,\mathrm{fm}^{-3}\,] = 0.191 - 0.0388((\gamma_0 - 0.387)^2 + (\gamma_1 - 0.387)^2)\,. \qquad (8)$$

Note that the maximal saturation density $\rho_0^{\max} = 0.191\,\mathrm{fm}^{-3}$ possible in the present perturbative calculation lies just at the upper end of the range $\rho_0 = (0.166 \pm 0.027)\,\mathrm{fm}^{-3}$ quoted in ref. [19]. Interestingly, the maximal saturation density $\rho_0^{\max} = 0.191\,\mathrm{fm}^{-3}$ is reached in the near vicinity of the special point $\gamma_0 = \gamma_1 = 1/2$. The

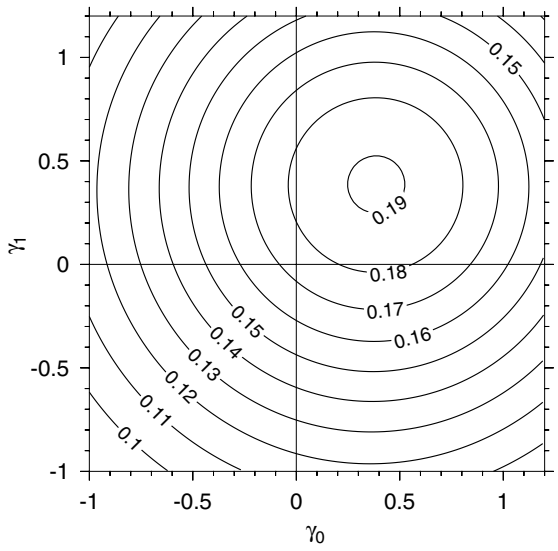

Fig. 3. Contours of constant nuclear-matter saturation density ρ_0 (in units of fm^{-3}) in the (γ_0, γ_1)-plane of short-range parameters. The maximal saturation density is $\rho_0^{\max} = 0.191\ \mathrm{fm}^{-3} \simeq 1.15\rho_0^{\mathrm{emp}}$. The binding energy per particle is fixed to the value $-\bar{E}(k_{f0}) = 15.3\,\mathrm{MeV}$.

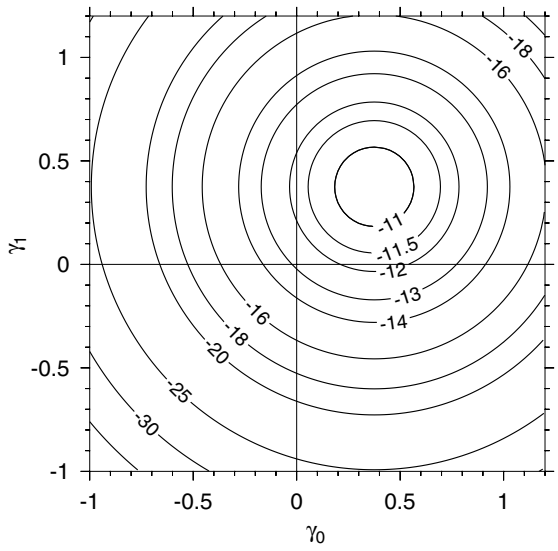

Fig. 4. Contours of constant saturation energy $\bar{E}(k_{f0})$ (in units of MeV) in the (γ_0, γ_1)-plane of short-range parameters. The maximal saturation energy is $\bar{E}(k_{f0})^{\max} = -10.7\,\mathrm{MeV}$. The nuclear-matter saturation density is fixed to the value $\rho_0 = 0.158\,\mathrm{fm}^{-3}$ [22].

latter describes the situation in which the (explicitly introduced) short-range NN-interaction exactly cancels the contact pieces of the 1π-exchange. The additional constraint $\gamma_1 = -0.75$ taken over from the fit to the neutron matter equation of state (see sect. 2) leads (together with $\gamma_0 = 0.39$) however to a somewhat too low saturation density of $\rho_0 = 0.134\,\mathrm{fm}^{-3}$. The other parameter $\mathit{\Gamma}_0 = 5.63$ needed to keep the depth of the saturation curve at $-15.3\,\mathrm{MeV}$ translates into an isospin-0 cut-off of $\mathit{\Lambda}_0 = 0.55\,\mathrm{GeV}$. Its value does not differ much from the isospin-1 cut-off $\mathit{\Lambda}_1 \simeq 0.48\,\mathrm{GeV}$ needed for the neutron matter equation of state and it also lies within the physically acceptable range. Note that momentum cut-offs around 0.5 GeV have also been used in chiral perturbation theory calculations of NN-phase shifts in refs. [20,21]. In these works the cut-off serves the somewhat different purpose of regulating the (non-perturbative) Lippmann-Schwinger equation. However, no comparable fine-tuning of $\mathit{\Lambda}$ is needed in these works since the cut-off dependence of NN-observables can to a large extent be balanced by the strengths of NN-contact terms.

One may also invert the fitting procedure and extract this way the parameter dependence of the maximal binding energy $-\bar{E}(k_{f0})$ per nucleon at fixed saturation density ρ_0. For this purpose we choose the value $\rho_0 = 0.158\,\mathrm{fm}^{-3}$ as obtained by extrapolation from inelastic electron scattering off heavy nuclei [22]. Figure 4 shows the resulting contours of constant saturation energy $\bar{E}(k_{f0})$ in the (γ_0, γ_1)-plane of short-range parameters. Again, to a good approximation these contours are concentric circles around the point $\gamma_0 = \gamma_1 = 0.38$ in parameter space where the saturation energy becomes maximal, $\bar{E}(k_{f0})^{\max} = -10.7\,\mathrm{MeV}$.

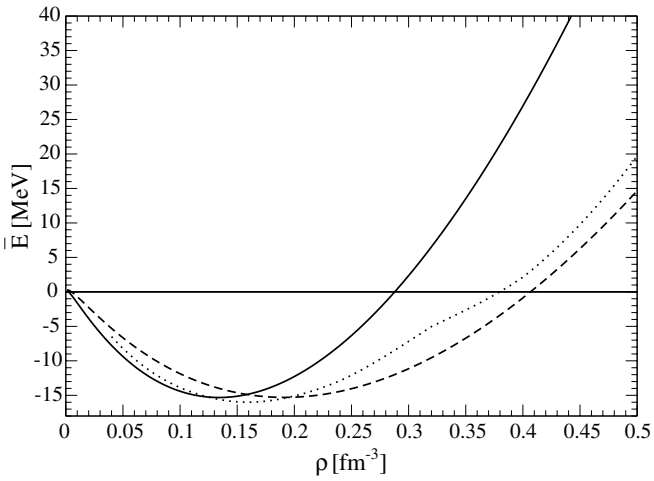

Fig. 5. The energy per particle $\bar{E}(k_f)$ of isospin-symmetric nuclear-matter *versus* the nucleon density $\rho = 2k_f^3/3\pi^2$. The full curve corresponds to the parameter set constrained by the neutron matter equation of state. The dashed curve shows the case of maximal saturation density $\rho_0^{\max} = 0.191\ \mathrm{fm}^{-3}$. The dotted line stems from the many-body calculation of the Urbana group [1].

The full curve in fig. 5 shows the equation of state of isospin-symmetric nuclear matter corresponding to the parameter set ($\gamma_0 = 0.39$, $\gamma_1 = -0.75$, $\mathit{\Gamma}_0 = 5.63$, $\mathit{\Gamma}_1 = 2.76$) constrained by the equation of state of pure neutron matter. The nuclear-matter compressibility (related to the curvature of the saturation curve at its minimum) comes out as $K = k_{f0}^2 \bar{E}''(k_{f0}) = 243\,\mathrm{MeV}$, in good agreement with the presently accepted empirical value $K = (250 \pm 25)\,\mathrm{MeV}$ [19,23]. For comparison, the value

$K = 253\,\mathrm{MeV}$ [10] of the nuclear-matter compressibility is obtained if the (explicit) short-range NN-terms are switched off ($\gamma_0 = \gamma_1 = 0$, $\Lambda_0 = \Lambda_1 = 0.61\,\mathrm{GeV}$). The dashed line in fig. 5 shows the equation of state $\bar{E}(k_f)$ with maximal saturation density $\rho_0^{\max} = 0.191\,\mathrm{fm}^{-3}$ which is realized by the parameter choice: $\gamma_0 = \gamma_1 = 0.39$ and $\Gamma_0 + \Gamma_1 = 6.46$ (or equivalently $\Lambda_0 = \Lambda_1 = 0.60\,\mathrm{GeV}$). In this case the nuclear-matter compressibility changes only slightly to $K = 250\,\mathrm{MeV}$. The dotted line in fig. 5 stems from the sophisticated many-body calculation of the Urbana group [1] using the Argonne V18 NN-potential plus boost corrections and three-nucleon interactions. By giving up the constraints from the neutron matter equation of state one could also reproduce this curve (for moderate densities $\rho \leq 0.3\,\mathrm{fm}^{-3}$). The corresponding best-fit parameters would be $\gamma_0 = \gamma_1 = -0.19$ and $\Lambda_0 = \Lambda_1 = 0.59\,\mathrm{GeV}$. Altogether, it seems that most of the parameter freedom of our calculation is already exhausted by adjusting the nuclear-matter saturation point. The compressibility is rather stable and takes on reasonable values around $K \simeq 250\,\mathrm{MeV}$.

4 Real single-particle potential

Next, we turn to the real part of the single-particle potential $U(p, k_f)$ below the Fermi surface ($p < k_f$). As outlined in ref. [9], the contributions to the (real) nuclear mean-field $U(p, k_f)$ can be classified as two-body and three-body potentials. The first diagram in fig. 1 (combined with all cut-off–dependent terms from iterated diagrams) leads to a momentum-independent contribution to the two-body potential of the form

$$U_2(p, k_f) = -\frac{(\Gamma_0 + \Gamma_1) g_A^2 k_f^3}{2(2\pi f_\pi)^2}\,, \tag{9}$$

which is just twice the energy per particle written in eq. (5). From the second pion-exchange diagram in fig. 1 one derives a (finite) contribution to the two-body potential of the form

$$\begin{aligned} U_2(p, k_f) &= \frac{(\gamma_0 + \gamma_1) g_A^4 M m_\pi^4}{(4\pi)^3 f_\pi^4} \\ &\times \Big\{ u + \frac{1}{8x}(1 + 3u^2 - 3x^2) \ln \frac{1 + (u+x)^2}{1 + (u-x)^2} \\ &+ \frac{1}{4x}(x^3 - 3x - 3u^2 x - 2u^3) \arctan(u+x) \\ &+ \frac{1}{4x}(x^3 - 3x - 3u^2 x + 2u^3) \arctan(u-x) \Big\}, \end{aligned} \tag{10}$$

with the abbreviation $x = p/m_\pi$. The second and third diagram in fig. 1 give each rise to three different contributions to the three-body potential. Altogether, they read

$$\begin{aligned} U_3(p, k_f) &= \frac{3(\gamma_0 + \gamma_1) g_A^4 M m_\pi^4}{(4\pi f_\pi)^4} \\ &\times \int_{-1}^{1} \mathrm{d}y \Big\{ \Big[uxy + (u^2 - x^2 y^2) \frac{H}{2} \Big] \Big[(r-1)s^2 + \ln(1+s^2) \Big] \\ &+ \int_{-xy}^{s-xy} \mathrm{d}\xi \left[2u\xi + (u^2 - \xi^2) \ln \frac{u+\xi}{u-\xi} \right] \\ &\times \frac{r(xy+\xi) + (r-1)(xy+\xi)^3}{1 + (xy+\xi)^2} + \int_0^u \mathrm{d}\xi\, \frac{\xi^2}{x} \\ &\times \Big[(r-1)\sigma^2 + \ln(1+\sigma^2) \Big] \ln \frac{|x+\xi y|}{|x-\xi y|} \Big\}, \end{aligned} \tag{11}$$

with the auxiliary function $\sigma = \xi y + \sqrt{u^2 - \xi^2 + \xi^2 y^2}$ and the ratio of parameters $r = (\gamma_0^2 + \gamma_1^2)/(\gamma_0 + \gamma_1)$. The real single-particle potential $U(p, k_f)$ is completed by adding to the terms eqs. (9)-(11) the contributions from 1π-exchange and iterated 1π-exchange written down in eqs. (8)-(13) of ref. [9]. Again, the higher-order relativistic $1/M^2$-correction to 1π-exchange (see eq. (8) in ref. [9]) is neglected here for reasons of consistency.

The slope of the real single-particle potential $U(p, k_f)$ at the Fermi surface $p = k_f$ determines the effective nucleon mass (the product of "k-mass" and "E-mass" divided by the free mass in the nomenclature of ref. [24]) via the relation $M^*(k_f) = M/(1 + B - k_f^2/2M^2)$. For the slope parameter B we find the following numerical result (choosing $k_f = 2m_\pi$):

$$\begin{aligned} B = \frac{M}{p} \frac{\partial U(p, k_f)}{\partial p}\bigg|_{p = k_f = 2m_\pi} = \\ -0.239 - 1.245\big((\gamma_0 - 0.388)^2 + (\gamma_1 - 0.388)^2\big)\,. \end{aligned} \tag{12}$$

The negative coefficient in front of the quadratic polynomial in γ_0 and γ_1 is known analytically from Galitskii's calculation [25,26] and it reads in our notation: $g_A^4 M^2 k_f^2 (1 - 7\ln 2)/(80\pi^4 f_\pi^4)$. One deduces from eq. (12) that the slope parameter B is negative definite. This implies that according to our calculation the effective nucleon mass at the Fermi surface $M^*(k_{f0})$ is always larger than the free nucleon mass $M = 939\,\mathrm{MeV}$. While the iteration of 1π-exchange with the NN-contact vertex (second diagram in fig. 1 being linear in $\gamma_0 + \gamma_1$) can of course reduce the effective nucleon mass, there are counteracting quadratic effects from the iteration of the NN-contact interaction with itself, which set a limit to this. The lower bound on the effective nucleon mass in the present calculation is $M^*(k_{f0}) \geq 1.4M$. It exceeds considerably the value $M^*(k_{f0}) \simeq 1.15M$ found in the self-consistent Brueckner calculation of ref. [27] (see fig. 6 therein). Interestingly, the parameter set ($\gamma_0 = \gamma_1 = 0.39$) leading to the minimal effective nucleon mass coincides with that of maximal saturation density $\rho_0^{\max} = 0.191\,\mathrm{fm}^{-3}$. Both features occur simultaneously in a situation where the (explicitly introduced) short-range NN-interaction cancels almost completely the contact piece of the 1π-exchange.

The lower curve in fig. 6 shows the real part of the single-particle potential $U(p, k_{f0})$ at saturation density

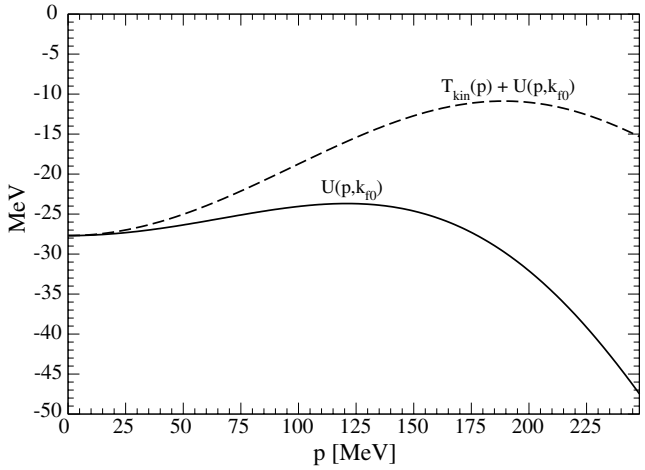

Fig. 6. The lower curve shows the real part of the single-particle potential $U(p, k_{f0})$ at saturation density $k_{f0} = 248\,\mathrm{MeV}$ for the parameter set constrained by the equation of state of pure neutron matter. The upper curve includes the relativistically improved kinetic energy $T_{\rm kin}(p) = p^2/2M - p^4/8M^3$.

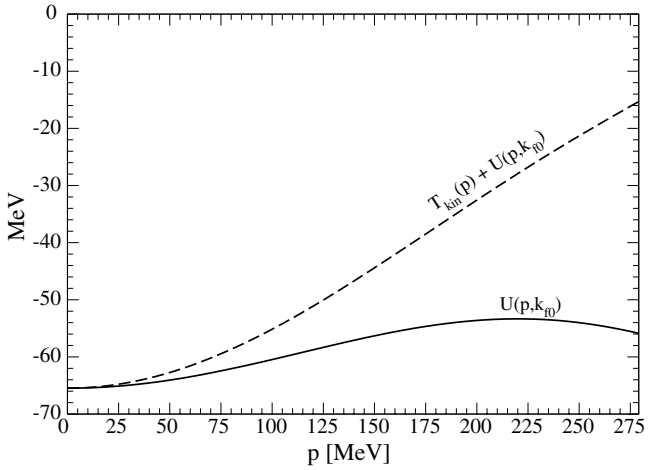

Fig. 7. The lower curve shows the real part of the single-particle potential $U(p, k_{f0})$ at $k_{f0} = 279\,\mathrm{MeV}$ for the case of maximal saturation density $\rho_0^{\max} = 0.191\,\mathrm{fm}^{-3}$. The upper curve includes the relativistically improved kinetic energy $T_{\rm kin}(p) = p^2/2M - p^4/8M^3$.

$k_{f0} = 248\,\mathrm{MeV}$ for the parameter set constrained by the equation of state of pure neutron matter. The potential depth of $U(0, k_{f0}) = -27.7\,\mathrm{MeV}$ is by far too weakly attractive, *i.e.* at least a factor of two too small. Moreover, a very strong decrease of $U(0, k_{f0})$ sets in above $p = k_{f0}/2 = 124\,\mathrm{MeV}$. The consequence of this behavior is that the total single-particle energy $T_{\rm kin}(p) + U(p, k_{f0})$, shown by the dashed line in fig. 6, does not rise monotonically with the nucleon momentum p. From that perspective the single-particle potential $U(p, k_{f0})$ presented in fig. 6 is as unrealistic as the one in the scheme of Lutz *et al.* [7,10]. The requirements of a good neutron matter equation of state and good single-particle properties in isospin-symmetric nuclear matter cannot be fulfilled simultaneously in a calculation to fourth order. A possible remedy of this could be a p^2-dependent NN-contact interaction (contributing at fifth order in small momenta).

The lower curve in fig. 7 shows the real part of the single-particle potential $U(p, k_{f0})$ for the case of maximal saturation density $\rho_0^{\max} = 0.191\,\mathrm{fm}^{-3}$. The potential depth of $U(p, k_{f0}) = -65.5\,\mathrm{MeV}$ is now close to the value $-64\,\mathrm{MeV}$ obtained in the calculation of ref. [27] using the Paris NN-potential. The momentum dependence is also reasonable since it leads to a monotonic rise of the total single-particle energy $T_{\rm kin}(p) + U(p, k_{f0})$, as it should be. Note that both dashed curves in figs. 6, 7 end at the Fermi surface $p = k_{f0}$ with the value $\bar{E}(k_{f0}) = -15.3\,\mathrm{MeV}$ as required by the Hugenholtz-Van-Hove theorem [28]. This serves an important check on our (analytical and numerical) calculations.

5 Imaginary single-particle potential

Next, we come to the imaginary single-particle potential $W(p, k_f)$ as it arises from the iteration of the NN-contact interaction with 1π-exchange and with itself. For $p \le k_f$ the imaginary single-particle potential $W(p, k_f)$ is equal to the half-width of nucleon-hole states in the Fermi sea. As outlined in ref. [9] the contributions to $W(p, k_f)$ can be classified as two-body, three-body and four-body terms. From a technical point of view a ν-body term involves an integral over the product of $\nu - 1$ Fermi spheres of radius k_f. The second and third diagram in fig. 1 give rise to a two-body term of the form

$$W_2(p,k_f) = \frac{(\gamma_0+\gamma_1) g_A^4 M m_\pi^4}{(8\pi)^3 f_\pi^4} \times \bigg\{ (r-1)\bigg(\frac{x^4}{5} - 2u^2x^2 - 3u^4\bigg) + 4 + 14u^2 - \frac{22x^2}{3} + \frac{2}{x}(3x^2 - 3u^2 - 1)\Big[\arctan(u+x) - \arctan(u-x)\Big] + \frac{1}{x}(x^3 - 3u^2x - 3x - 2u^3)\ln[1+(u+x)^2] + \frac{1}{x}(x^3 - 3u^2x - 3x + 2u^3)\ln[1+(u-x)^2]\bigg\}, \qquad (13)$$

with the coefficient r defined after eq. (11). The associated three-body term reads

$$W_3(p,k_f) = \frac{(\gamma_0+\gamma_1) g_A^4 M m_\pi^4}{(8\pi)^3 f_\pi^4} \times \bigg\{ 4(r-1)(3u^4 - x^4) + \frac{41x^2}{3} - 31u^2 - 5 - (u^2-x^2)^2 - 3\ln(1+4x^2) + \bigg(6x - \frac{3}{2x}\bigg)\arctan 2x$$

$$+\Big[\arctan(u+x)-\arctan(u-x)\Big]$$
$$\times\frac{1}{2x}\Big[(u^2-x^2)^3+(12u^2+27)(u^2-x^2)+8\Big]$$
$$+\Big(6+9u^2-3x^2+\frac{2u^3}{x}\Big)\ln[1+(u+x)^2]$$
$$+\Big(6+9u^2-3x^2-\frac{2u^3}{x}\Big)\ln[1+(u-x)^2]\Big\}, \quad (14)$$

and the four-body term is given by the expression

$$W_4(p,k_f)=\frac{(\gamma_0+\gamma_1)g_A^4Mm_\pi^4}{(8\pi)^3f_\pi^4}$$
$$\times\Big\{2(r-1)\Big(\frac{17x^4}{5}-3u^4-2u^2x^2\Big)+1+20u^2-\frac{28x^2}{3}$$
$$+6\ln(1+4x^2)+\Big(\frac{3}{x}-12x\Big)\arctan 2x$$
$$+\Big[\arctan(u+x)-\arctan(u-x)\Big]\frac{1}{2x}\Big[(x^2-u^2)^3+3x^4$$
$$+6u^2x^2-9u^4+27x^2-15u^2-7\Big]+2(x^2-3u^2-3)$$
$$\times\ln\Big([1+(u+x)^2][1+(u-x)^2]\Big)+(u^2-x^2)^2\Big\}. \quad (15)$$

The additional contributions to $W(p,k_f)$ from the iterated 1π-exchange Hartree and Fock diagrams are collected in eqs. (20)-(25) of ref. [9]. In the appendix we present also novel analytical expressions for the three-body and four-body Hartree term of iterated 1π-exchange. The total imaginary single-particle potential evaluated at zero nucleon momentum ($p=0$) can even be written as a closed-form expression:

$$W(0,k_f)=\frac{3\pi g_A^4Mm_\pi^4}{(4\pi f_\pi)^4}\Big\{\Big[3+2(\gamma_0^2+\gamma_1^2-\gamma_0-\gamma_1)\Big]\frac{u^4}{4}$$
$$+(\gamma_0+\gamma_1-3)u^2-\frac{2u^2}{1+u^2}+\frac{\pi^2}{12}+\mathrm{Li}_2(-1-u^2)$$
$$+\Big[5-\gamma_0-\gamma_1+\ln(2+u^2)-\frac{1}{2}\ln(1+u^2)\Big]\ln(1+u^2)\Big\}, \quad (16)$$

where $\mathrm{Li}_2(-a^{-1})=\int_0^1 \mathrm{d}\zeta\,(\zeta+a)^{-1}\ln\zeta$ denotes the conventional dilogarithmic function. Note that eq. (16) determines the density dependence of the half-width of nucleon-hole states at the bottom of the Fermi sea.

Figure 8 shows the imaginary single-particle potential $W(p,k_{f0})$ at saturation density as a function of the nucleon momentum p. The full curve corresponds to the parameter set constrained by the neutron matter equation of state (where $k_{f0}=248\,\mathrm{MeV}$). The resulting value $W(0,k_{f0})=43.3\,\mathrm{MeV}$ is somewhat larger than the value $W(0,k_{f0})\simeq 40\,\mathrm{MeV}$ obtained in the self-consistent Brueckner calculation of ref. [27] using the phenomenological Paris *NN*-potential. The dashed curve in fig. 8 shows the case of maximal saturation density $\rho_0^{\max}=0.191\ \mathrm{fm}^{-3}$. With associated parameters $\gamma_0=\gamma_1=0.39$ the imaginary single-particle potential at $p=0$ comes out as $W(0,k_{f0})=22.7\,\mathrm{MeV}$. This value is close to the result $W(0,k_{f0})\simeq 20\,\mathrm{MeV}$ found in the calculation of ref. [29] employing the Gogny D1 effective interaction. For comparison, the value $W(0,k_{f0})=29.7\,\mathrm{MeV}$ [9] results from the pure pion-exchange dynamics. The momentum dependence of $W(p,k_{f0})$ is generic. As a consequence of the decreasing phase space available for redistributing the nucleon-hole state energy the curves in fig. 8 drop with momentum p and $W(p,k_{f0})$ reaches zero at the Fermi surface $p=k_{f0}$. According to Luttinger's theorem [30] this vanishing is of quadratic order, $W(p,k_f)\sim(p-k_f)^2$, a feature which is clearly exhibited by the curves in fig. 8.

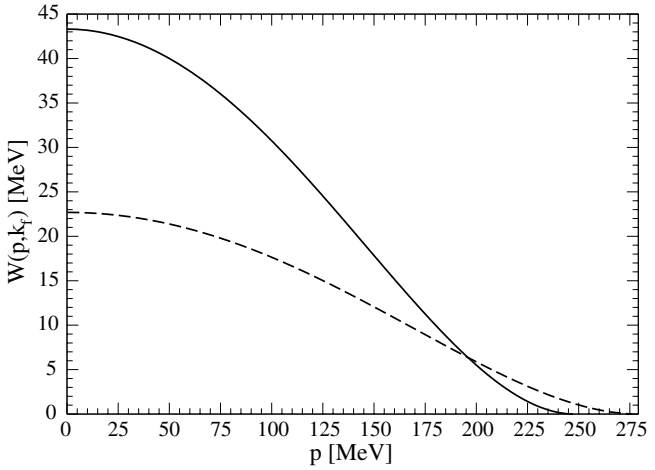

Fig. 8. The imaginary single-particle potential $W(p,k_{f0})$ at saturation density *versus* the nucleon momentum p. The full curve corresponds to the parameter set constrained by the neutron matter equation of state. The dashed curve shows the case of maximal saturation density $\rho_0^{\max}=0.191\ \mathrm{fm}^{-3}$.

6 Asymmetry energy

This section is devoted to the density-dependent asymmetry energy $A(k_f)$. The asymmetry energy is generally defined by the expansion of the energy per particle of isospin-asymmetric nuclear matter (described by different proton and neutron Fermi momenta $k_{p,n}=k_f(1\mp\delta)^{1/3}$) around the symmetry line: $\bar{E}_{\mathrm{as}}(k_p,k_n)=\bar{E}(k_f)+\delta^2\,A(k_f)+\mathcal{O}(\delta^4)$. Evaluating the first diagram in fig. 1 and combining that partial result with all cut-off–dependent terms from iterated diagrams, one obtains the following contribution (linear in density) to the asymmetry energy:

$$A(k_f)=\frac{g_A^2k_f^3}{3(4\pi f_\pi)^2}(3\Gamma_0-\Gamma_1)\,, \quad (17)$$

with the parameters Γ_0 and Γ_1 defined in eqs. (2), (5). From the second pion-exchange diagram in fig. 1 with two medium insertions on parallel nucleon lines one gets a

(finite) contribution to the asymmetry energy of the form

$$A(k_f) = \frac{g_A^4 M m_\pi^4}{3(8\pi)^3 f_\pi^4}\bigg\{2(\gamma_0+\gamma_1)u + 16\gamma_0 u^2 \arctan 2u - \bigg[(6\gamma_0+2\gamma_1)u + \frac{\gamma_0+\gamma_1}{2u}\bigg]\ln(1+4u^2)\bigg\}. \quad (18)$$

The same (pion-exchange) diagram with three medium insertions gives rise to a contribution to the asymmetry energy which can be represented as a double integral:

$$\begin{aligned} A(k_f) = {} & \frac{g_A^4 M m_\pi^4}{(4\pi f_\pi)^4 u^3}\int_0^u \mathrm{d}x\, x^2 \int_{-1}^1 \mathrm{d}y \bigg\{(\gamma_0+\gamma_1) \\ & \times\bigg\{\bigg[\frac{uxy(11u^2-15x^2y^2)}{3(u^2-x^2y^2)} + (u^2-5x^2y^2)\frac{H}{2}\bigg] \\ & \times\Big[\ln(1+s^2)-s^2\Big] + \frac{4u^2s^4H}{3(1+s^2)} + \frac{s^2}{6(1+s^2)^2} \\ & \times\Big[2uxy + (u^2-x^2y^2)H\Big]\Big[8s(1+s^2)(5s'-3s-s'') \\ & +(3+s^2)(8ss'-3s^2-8s'^2)\Big]\bigg\} \\ & +4\gamma_1 u^2\bigg[\frac{2uxy[\ln(1+s^2)-s^2]}{3(u^2-x^2y^2)} \\ & +\bigg(\ln(1+s^2) - \frac{s^2(3+5s^2)}{3(1+s^2)}\bigg)H\bigg]\bigg\}, \end{aligned} \quad (19)$$

with $s' = u\,\partial s/\partial u$ and $s'' = u^2\,\partial^2 s/\partial u^2$ denoting partial derivatives. In the case of the third diagram in fig. 1 with three medium insertions the occurring double integral can actually be solved. The k_f^4-contribution to the asymmetry energy originating from the iterated NN-contact interaction reads

$$A(k_f) = \Big(\frac{g_A k_f}{2\pi f_\pi}\Big)^4 \frac{M}{15}\Big[\gamma_1^2(3-\ln 2) - \gamma_0^2(2+\ln 2)\Big]. \quad (20)$$

The absence of an interference term proportional to $\gamma_0\gamma_1$ is highly remarkable. The asymmetry energy $A(k_f)$ is completed by adding to the terms in eqs. (17)-(20) the contributions from the (relativistically improved) kinetic energy, (static) 1π-exchange and iterated 1π-exchange written down in eqs. (20)-(26) of ref. [8].

In fig. 9, we show the asymmetry energy $A(k_f)$ *versus* the nucleon density $\rho = 2k_f^3/3\pi^2$. The full curve corresponds to the parameter set constrained by the neutron matter equation of state. The predicted value of the asymmetry energy at saturation density $\rho_0 = 0.134\,\mathrm{fm}^{-3}$ is $A(k_{f0}) = 30.8\,\mathrm{MeV}$. This is close to the empirical value $A(k_{f0}) \simeq 33\,\mathrm{MeV}$ of ref. [18] obtained in extensive fits to nuclide masses. As a consequence of the built-in constraints from the neutron matter equation of state the full curve in fig. 9 starts to bend downwards only above relatively high densities $\rho > 0.3\,\mathrm{fm}^{-3}$. The dashed curve in fig. 9 shows the case of maximal saturation density $\rho_0^{\max} = 0.191\ \mathrm{fm}^{-3}$ realized by the parameters $\gamma_0 = \gamma_1 = 0.39$. We use furthermore the decomposition[3]

[3] Returning to eq. (2) one notices that Γ_1 and γ_1 are necessarily approximately equal if $\gamma_1 \approx 1/2$.

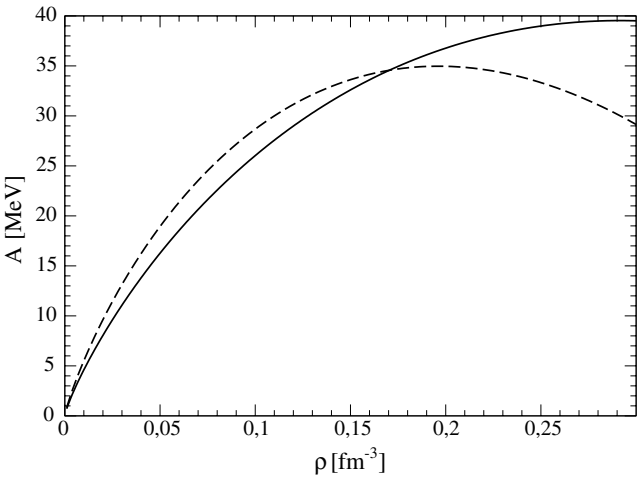

Fig. 9. The asymmetry energy $A(k_f)$ *versus* the nucleon density $\rho = 2k_f^3/3\pi^2$. The full curve corresponds to the parameter set constrained by the neutron matter equation of state. The dashed curve shows the case of maximal saturation density $\rho_0^{\max} = 0.191\ \mathrm{fm}^{-3}$.

$\Gamma_0 + \Gamma_1 = 6.04 + 0.42$ as it follows from choosing a common cut-off $\Lambda_0 = \Lambda_1 = 0.60\,\mathrm{GeV}$. The resulting value $A(k_{f0}) = 35.0\,\mathrm{MeV}$ of the asymmetry energy at saturation density $\rho_0^{\max} = 0.191\,\mathrm{fm}^{-3}$ is also in good agreement with the empirical value. However, in that case the downward bending of $A(k_f)$ sets in immediately above saturation density. The situation concerning the high-density behavior of the asymmetry energy is still controversial. While Brueckner-Hartree-Fock calculations of ref. [31] predict a monotonic increase with density the results of the Urbana group [16] show a downward bending of $A(k_f)$ at densities $\rho = 0.4\,\mathrm{fm}^{-3}$ or higher (see fig. 8 therein). Altogether, it seems that the value of the asymmetry at saturation density is rather stable while the detailed density dependence of $A(k_f)$ reflects more pronouncedly some properties of the corresponding neutron matter equation of state.

7 Nuclear matter at finite temperatures

In this section, we discuss nuclear matter at finite temperatures $T \leq 30\,\mathrm{MeV}$. We are particularly interested in the first-order liquid-gas phase transition of isospin-symmetric nuclear matter and its associated critical point $(\rho_\mathrm{c}, T_\mathrm{c})$. As outlined in ref. [13], a thermodynamically consistent extension of the present (perturbative) calculational scheme to finite temperatures is to relate it directly to the free energy per particle $\bar{F}(\rho, T)$, whose natural thermodynamical variables are the nucleon density ρ and the temperature T. In that case the free energy density $\rho\bar{F}(\rho, T)$ of isospin-symmetric nuclear matter consists of a sum of convolution integrals over interaction kernels $\mathcal{K}_j$ multiplied by powers of the density of nucleon states in momentum space:

$$d(p_j) = \frac{p_j}{2\pi^2}\bigg[1 + \exp\frac{p_j^2 - 2M\tilde{\mu}}{2MT}\bigg]^{-1}. \quad (21)$$

The effective one-body "chemical potential" $\tilde{\mu}(\rho,T)$ entering the Fermi-Dirac distribution in eq. (21) is determined by the relation to the particle density $\rho = 4\int_0^\infty \mathrm{d}p_1\, p_1 d(p_1)$. We now write down the additional interaction kernels arising from the *NN*-contact interaction proportional to $\gamma_{0,1}$. The contact interaction at first order and the cut-off–dependent pieces from iterated diagrams are summed up via the parameters $\mathit{\Gamma}_{0,1}$. Their contribution to the two-body kernel reads

$$\mathcal{K}_2^{(\mathit{\Gamma})} = -\frac{3g_A^2}{2f_\pi^2}(\mathit{\Gamma}_0+\mathit{\Gamma}_1)p_1p_2\,. \tag{22}$$

Obviously, this kernel generates a temperature-independent contribution to the free energy per particle which just grows linear in density, $\bar{F}(\rho,T)\sim\rho$. From the second pion-exchange diagram in fig. 1 one derives a further (finite) contribution to the two-body kernel of the form

$$\begin{aligned}\mathcal{K}_2^{(\gamma)} = \frac{3(\gamma_0+\gamma_1)g_A^4 M m_\pi^2}{64\pi f_\pi^4}\Bigg\{ & m_\pi \ln\frac{m_\pi^2+(p_1+p_2)^2}{m_\pi^2+(p_1-p_2)^2} \\ & -2(p_1+p_2)\arctan\frac{p_1+p_2}{m_\pi} \\ & +2(p_1-p_2)\arctan\frac{p_1-p_2}{m_\pi}\Bigg\}. \end{aligned}\tag{23}$$

Temperature and density Pauli-blocking effects in intermediate *NN*-states are incorporated in the three-body kernel $\mathcal{K}_3$. The second and third diagram in fig. 1 together give rise to the following contribution to the three-body kernel:

$$\begin{aligned}\mathcal{K}_3^{(\gamma)} = \frac{3g_A^4 M}{8f_\pi^4}\int_{|p_1-p_2|}^{p_1+p_2}\mathrm{d}q\left[\gamma_0^2+\gamma_1^2-\frac{(\gamma_0+\gamma_1)q^2}{m_\pi^2+q^2}\right] \\ \times\ln\frac{|p_1^2-p_2^2+q^2+2p_3q|}{|p_1^2-p_2^2+q^2-2p_3q|}\,. \end{aligned}\tag{24}$$

The remaining kernels building up the free nucleon gas part and the interaction contributions from 1π-exchange and iterated 1π-exchange are written down in eqs. (4)-(7), (11), (12) of ref. [13]. Again, the (higher-order) relativistic $1/M^2$-correction to the 1π-exchange two-body kernel $\mathcal{K}_2^{(1\pi)}$ (see eq. (5) in ref. [13]) is neglected here for reasons of consistency. A special feature of the finite-temperature formalism is the so-called anomalous contribution $\rho\bar{\mathcal{A}}(\rho,T)$ with no counterpart in the calculation to the ground-state energy density $\rho\bar{E}(k_f)$ at $T=0$ [32, 33]. The basic physical mechanism behind this "anomalous" contribution is the possibility of interactions between particles and holes of the same momentum at finite temperature. From the combination of pion-exchange and zero-range *NN*-contact interaction we derive the following anomalous contribution to the free energy per particle of isospin-symmetric nuclear matter:

$$\begin{aligned}\bar{\mathcal{A}}(\rho,T) = & -\frac{[\mathit{\Omega}_1'(\rho,T)]^2}{2\rho\,\mathit{\Omega}_0''(\rho,T)} + \frac{9g_A^4}{8f_\pi^4 T\rho} \\ & \times\int_0^\infty\mathrm{d}p_1\int_0^\infty\mathrm{d}p_2\int_0^\infty\mathrm{d}p_3\, d(p_1)d(p_2)[2\pi^2 d(p_2)-p_2]d(p_3) \\ & \times\left[(\gamma_0+\gamma_1-1)p_1+\frac{m_\pi^2}{4p_2}\ln\frac{m_\pi^2+(p_1+p_2)^2}{m_\pi^2+(p_1-p_2)^2}\right] \\ & \times\left[(\gamma_0+\gamma_1-1)p_3+\frac{m_\pi^2}{4p_2}\ln\frac{m_\pi^2+(p_3+p_2)^2}{m_\pi^2+(p_3-p_2)^2}\right], \end{aligned}\tag{25}$$

with the $\tilde{\mu}$-derivative of the grand canonical potential due to static 1π-exchange and the *NN*-contact coupling:

$$\begin{aligned}\mathit{\Omega}_1'(\rho,T) = & \frac{3g_A^2 M}{2f_\pi^2}\int_0^\infty\mathrm{d}p_1\int_0^\infty\mathrm{d}p_2\; d(p_1)\frac{d(p_2)}{p_2} \\ & \times\left[\frac{(p_1+p_2)^3}{m_\pi^2+(p_1+p_2)^2}+\frac{(p_1-p_2)^3}{m_\pi^2+(p_1-p_2)^2}-2(\gamma_0+\gamma_1)p_1\right], \end{aligned}\tag{26}$$

and the second $\tilde{\mu}$-derivative of the free nucleon gas part:

$$\mathit{\Omega}_0''(\rho,T) = -4M\int_0^\infty\mathrm{d}p_1\;\frac{d(p_1)}{p_1}\,. \tag{27}$$

The first term in eq. (25) originates from taking into account the contributions of (static) 1π-exchange and the *NN*-contact coupling in the Legendre transformation from the grand canonical potential to the free energy density and from the perturbative shift of the chemical potential $\tilde{\mu}\to\tilde{\mu}-\mathit{\Omega}_1'(\rho,T)/\mathit{\Omega}_0''(\rho,T)$ (for details on that procedure, see ref. [33]). We have explicitly checked that the anomalous contribution vanishes identically at $T=0$ for all densities ρ. This vanishing, $\bar{\mathcal{A}}(\rho,0)=0$, is an automatic consequence of the Kohn-Luttinger-Ward theorem [33] which of course holds in our case since the Fermi surface and the *NN*-interactions are invariant under spatial rotations. Furthermore, it is interesting to observe that the temperature and density-dependent anomalous contribution $\bar{\mathcal{A}}(\rho,T)$ vanishes identically in the chiral limit $m_\pi=0$. The latter feature has the practical consequence that the behavior of nuclear matter at finite temperatures $T\leq 30\,\mathrm{MeV}$ is only marginally influenced by the anomalous contribution $\bar{\mathcal{A}}(\rho,T)$.

Figure 10 shows for the case of maximal saturation density ($\gamma_0=\gamma_1=0.39$) the calculated pressure isotherms $P(\rho,T)=\rho^2\partial\bar{F}(\rho,T)/\partial\rho$ of isospin-symmetric nuclear matter at four selected temperatures $T=0$, 15, 21, 25 MeV. As it should be, these curves display a first-order liquid-gas phase transition similar to that of the van der Waals gas. The coexistence region between the liquid and the gas phase (which has to be determined by the Maxwell construction) terminates at the critical temperature T_c. From there on the pressure isotherms $P(\rho,T)$ grow monotonically with the nucleon density ρ. We find here a critical temperature of $T_\mathrm{c}\simeq 21\,\mathrm{MeV}$. This is already compatible with the value $T_\mathrm{c}=(20\pm3)\,\mathrm{MeV}$ as extracted in ref. [34] from multi-fragmentation data in

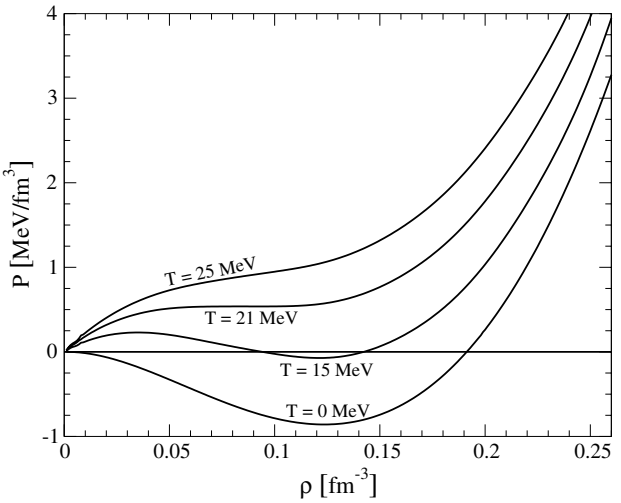

Fig. 10. Pressure isotherms $P(\rho, T)$ of isospin-symmetric nuclear matter for the case of maximal saturation density. The coexistence region of the liquid and gas phase ends at the critical point $\rho_c \simeq 0.09\,\mathrm{fm}^{-3}$ and $T_c \simeq 21\,\mathrm{MeV}$.

proton-on-gold collisions. Most other calculations get still lower values of the critical temperature, typically $T_c \simeq 18\,\mathrm{MeV}$ [15,35,36]. The reduction of T_c in comparison to $T_c \simeq 25.5\,\mathrm{MeV}$ obtained in ref. [13] from pion-exchange dynamics alone results from the less strong momentum dependence of the real single-particle potential $U(p, k_{f0})$ near the Fermi surface $p = k_{f0}$ (see fig. 7). As a general rule T_c grows with the effective nucleon mass $M^*(k_{f0})$ at the Fermi surface. Because of that property $T_c \simeq 21\,\mathrm{MeV}$ is the absolute minimum of the critical temperature possible within our perturbative calculation to fourth order.

For the parameter set ($\gamma_0 = 0.39$, $\gamma_1 = -0.75$) constrained by the equation of state of pure neutron matter the unrealistic momentum dependence of the associated real single-particle potential $U(p, k_{f0})$ (see fig. 6) ruins the behavior of nuclear matter at finite temperatures. The critical temperature of the liquid-gas phase transitions would lie in that case around $T_c \simeq 40\,\mathrm{MeV}$, thus exceeding realistic values by more than a factor of two.

Evidently, the single-particle properties around the Fermi surface are decisive for the thermal excitations and therefore they crucially influence the low-temperature behavior of nuclear matter.

8 Nuclear energy density functional

The energy density functional is a general starting point for nuclear-structure calculations within the framework of the self-consistent mean-field approximation [37]. In this context effective Skyrme forces [38–40] have gained much popularity because of their analytical simplicity and their ability to reproduce nuclear properties over the whole periodic table. In a recent work [41], we have calculated the nuclear energy density functional which emerges from (leading and next-to-leading order) chiral pion-nucleon dynamics. The calculation in ref. [41] included (only) the 1π-exchange Fock diagram and the iterated 1π-exchange Hartree and Fock diagrams. Therefore, the interest here is in the additional contributions from the NN-contact interaction appearing at the same order in the small momentum expansion.

Going up to quadratic order in spatial gradients (*i.e.* deviations from homogeneity) the energy density functional relevant for $N = Z$ even-even nuclei reads [41]

$$\mathcal{E}[\rho,\tau] = \rho\,\bar{E}(k_f) + \left[\tau - \frac{3}{5}\rho k_f^2\right] \times\left[\frac{1}{2M} - \frac{5k_f^2}{56M^3} + F_\tau(k_f)\right] + (\vec{\nabla}\rho)^2\,F_\nabla(k_f)\,, \quad (28)$$

with $\rho(\vec{r}) = 2k_f^3(\vec{r})/3\pi^2$ the local nucleon density (expressed in terms of a local Fermi momentum $k_f(\vec{r})$) and $\tau(\vec{r})$ the local kinetic-energy density. Note that we have left out in eq. (28) the spin-orbit coupling term since the NN-contact vertex proportional to $\gamma_{0,1}$ does not generate any contribution to it. The starting point for the construction of an explicit nuclear energy density functional $\mathcal{E}[\rho,\tau]$ is the bilocal density matrix as given by a sum over the occupied energy eigenfunctions: $\sum_{\alpha\in\mathrm{occ}}\Psi_\alpha(\vec{r}-\vec{a}/2)\Psi_\alpha^\dagger(\vec{r}+\vec{a}/2)$. According to Negele and Vautherin [42] it can be expanded in relative and center-of-mass coordinates, $\vec{a}$ and $\vec{r}$, with expansion coefficients determined by purely local quantities (nucleon density, kinetic-energy density and spin-orbit density). As outlined in sect. 2 of ref. [41] the Fourier transform of the (so-expanded) density matrix defines in momentum space a medium insertion for the inhomogeneous many-nucleon system:

$$\Gamma(\vec{p},\vec{q}) = \int \mathrm{d}^3r\, e^{-i\vec{q}\cdot\vec{r}}\,\theta(k_f - |\vec{p}\,|) \times\left\{1 + \frac{35\pi^2}{8k_f^7}(5\vec{p}^{\,2} - 3k_f^2)\left[\tau - \frac{3}{5}\rho k_f^2 - \frac{1}{4}\vec{\nabla}^2\rho\right]\right\}. \quad (29)$$

In comparison to eq. (5) in ref. [41] we have left out here the spin-dependent part (generating spin-orbit couplings) since it does not come into play. The strength function $F_\tau(k_f)$ in eq. (28) emerges via a perturbation on top of the density of states $\theta(k_f - |\vec{p}\,|)$. As a consequence of that $F_\tau(k_f)$ can be directly expressed in terms of the real single-particle potential $U(p, k_f)$ as

$$F_\tau(k_f) = \frac{35}{4k_f^7}\int_0^{k_f}\mathrm{d}p\,p^2(5p^2 - 3k_f^2)\,U(p,k_f)\,. \quad (30)$$

Note that any p-independent contribution, in particular the cut-off–dependent $\Gamma_{0,1}$-term in eq. (9), drops out. In the medium insertion eq. (29) $\tau - 3\rho k_f^2/5$ is accompanied by $-\vec{\nabla}^2\rho/4$. After performing a partial integration one is led to the following decomposition:

$$F_\nabla(k_f) = \frac{\pi^2}{8k_f^2}\,\frac{\partial F_\tau(k_f)}{\partial k_f} + F_d(k_f)\,, \quad (31)$$

where $F_d(k_f)$ comprises all those contributions for which the $(\nabla\rho)^2$-factor originates directly from the momentum

dependence of the interactions. We enumerate now the contributions to the strength functions $F_{\tau,d}(k_f)$ generated by the *NN*-contact vertex. From the second pion-exchange diagram in fig. 1 with two medium insertions we get

$$F_\tau(k_f) = \frac{(\gamma_0+\gamma_1)g_A^4 M m_\pi^2}{(8\pi)^3(uf_\pi)^4}\Big\{\Big(\frac{35u}{2}-\frac{63}{8u}-\frac{5}{16u^3}\Big) \times\ln(1+4u^2)+\frac{5}{4u}-\frac{117u}{2}-\frac{29u^3}{3} +\Big(4u^4+\frac{175}{4}\Big)\arctan 2u\Big\}, \tag{32}$$

$$F_d(k_f) = \frac{(\gamma_0+\gamma_1)g_A^4 M m_\pi}{4\pi(4f_\pi)^4(m_\pi^2+4k_f^2)}, \tag{33}$$

while the same diagram with three medium insertions gives

$$F_\tau(k_f) = \frac{35(\gamma_0+\gamma_1)g_A^4 M m_\pi^2}{(8\pi f_\pi)^4 u^7} \times\int_0^u \mathrm{d}x\, x^2\int_{-1}^1 \mathrm{d}y\Big\{20u^3xy[s^2-\ln(1+s^2)] +\Big[2uxy+(u^2-x^2y^2)H\Big]\Big[120xy\arctan s +40sxy(s^2-3)-15s^4+3(10+13u^2 -20x^2-5x^2y^2)[s^2-\ln(1+s^2)]\Big]\Big\}, \tag{34}$$

$$F_d(k_f) = -\frac{(\gamma_0+\gamma_1)g_A^4 M}{\pi^2 m_\pi(4uf_\pi)^4}\int_0^u \mathrm{d}x\, x^2\int_{-1}^1 \mathrm{d}y \times\Big\{\frac{Hs^2}{8(1+s^2)^3}(15+10s^2+3s^4) +\frac{uxys^2(3+s^2)}{4(u^2-x^2y^2)(1+s^2)^2}\Big\}. \tag{35}$$

In case of the last diagram in fig. 1 with three medium insertions we can even solve the integrals and get

$$F_\tau(k_f) = \frac{(\gamma_0^2+\gamma_1^2)g_A^4 M}{(2\pi f_\pi)^4}\,\frac{k_f^2}{108}(13-66\ln 2). \tag{36}$$

Evidently, there is no contribution to $F_d(k_f)$ from this last diagram since the *NN*-contact vertex is momentum independent. The additional contributions to $F_{\tau,d}(k_f)$ from 1π-exchange and iterated 1π-exchange can be found in sect. 3 of ref. [41].

The expression in eq. (28) multiplying the kinetic-energy density $\tau(\vec{r})$ has the interpretation of a reciprocal density-dependent effective nucleon mass:

$$\widetilde{M}^*(\rho) = M\Big[1-\frac{5k_f^2}{28M^2}+2M\,F_\tau(k_f)\Big]^{-1}. \tag{37}$$

In fig. 11, we show the ratio effective over free nucleon mass $\widetilde{M}^*(\rho)/M$ as a function of the nucleon density $\rho = 2k_f^3/3\pi^2$. The dashed curve shows the case of maximal saturation density $\rho_0^{\max} = 0.191\,\mathrm{fm}^{-3}$, while the dotted curve gives the result of the pion-exchange contributions alone [41]. As a consequence of the more moderate momentum dependence of the real single-particle potential $U(p,k_f)$ (see fig. 7) the effective nucleon mass $\widetilde{M}^*(\rho)$ is now reduced for all densities $\rho \le 3\rho_0/2$. In comparison to most (non-relativistic) mean-field calculations [38–40] the reduction by at most 15% as obtained here is a rather weak one. Note that the deviation of the effective nucleon mass $\widetilde{M}^*(\rho)$ from the free nucleon mass M does not just grow linear with density, but there are very strong curvature effects. This has mainly to do with the explicit presence of the small mass scale $m_\pi = 135\,\mathrm{MeV}$ in our calculation. For the parameter set ($\gamma_0 = 0.39$, $\gamma_1 = -0.75$) constrained by the neutron matter equation of state the unrealistic momentum dependence of the corresponding real single-particle potential $U(p,k_{f0})$ (see fig. 6) would even lead to a singularity of $\widetilde{M}^*(\rho)$ at $\rho \simeq 0.16\,\mathrm{fm}^{-3}$.

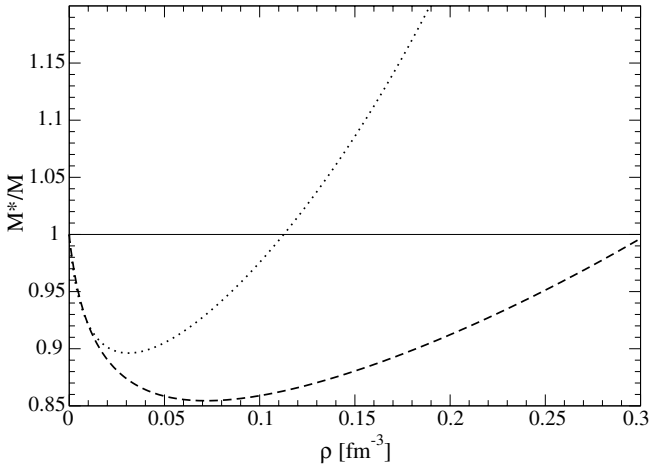

Fig. 11. The effective nucleon mass $\widetilde{M}^*(\rho)$ divided by the free nucleon mass M *versus* the nucleon density $\rho = 2k_f^3/3\pi^2$. The dashed curve shows the case of maximal saturation density $\rho_0^{\max} = 0.191\,\mathrm{fm}^{-3}$. The dotted curve gives the result of the pion-exchange contributions alone.

In fig. 12, we show the strength function $F_\nabla(k_f)$ related to the $(\vec{\nabla}\rho)^2$-term in the nuclear energy density functional *versus* the nucleon density $\rho = 2k_f^3/3\pi^2$. The full curve corresponds to the parameter set constrained by the neutron matter equation of state. The dashed curve shows the case of maximal saturation density $\rho_0^{\max} = 0.191\,\mathrm{fm}^{-3}$. For comparison, the dotted curve gives the result of the pion-exchange contributions alone [41]. The three horizontal lines represent the constant values $F_\nabla(k_f) = [9t_1 - (5+4x_2)t_2]/64$ of the Skyrme forces Sly [39], SIII [38] and MSk [40]. In the case of Sly and MSk we have performed averages over the various parameter sets Sly4-7 [39] and MSk1-6 [40]. One observes that in the case of maximal saturation density (dashed line in fig. 12) the effects from the *NN*-contact interaction move the prediction for $F_\nabla(k_f)$ further away from the empirical values. For the parameter set constrained by the neutron matter equation of state one gets from the *NN*-contact interaction a substantial lowering of the strength function $F_\nabla(k_f)$ compared to

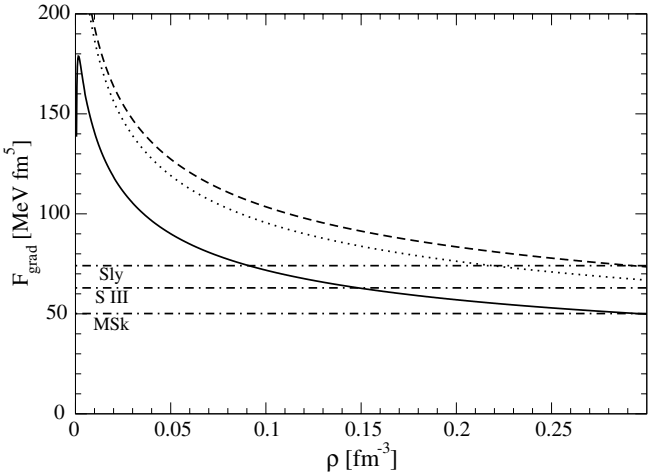

Fig. 12. The strength function $F_\nabla(k_f)$ related to the $(\vec{\nabla}\rho)^2$-term in the nuclear energy density functional *versus* the nucleon density $\rho = 2k_f^3/3\pi^2$. The full curve corresponds to the parameter set constrained by the neutron matter equation of state. The dashed curve shows the case of maximal saturation density $\rho_0^{\max} = 0.191$ fm^{-3}. The dotted curve gives the result of the pion-exchange contributions alone.

the pure pion-exchange contributions [41]. In the region $\rho_0/2 < \rho < 3\rho_0/2$ the prediction falls now into the empirically allowed band. The strong rise of $F_\nabla(k_f)$ at very low densities has to do with the presence of the small mass scale $m_\pi = 135\,\mathrm{MeV}$, and with associated chiral singularities (of the form m_π^{-2} and m_π^{-1}).

Altogether, one finds a conflicting situation concerning the effects of the NN-contact interaction on the strength functions $F_\tau(k_f)$ and $F_\nabla(k_f)$. The parameter set with an unrealistic p-dependence of single-particle potential $U(p,k_f)$, and therefore an unrealistic effective nucleon mass $\widetilde{M}^*(\rho)$, leads to an improved description of the strength function $F_\nabla(k_f)$ related to the $(\vec{\nabla}\rho)^2$-term in the nuclear energy density functional. The inclusion of short-range NN-terms does therefore not lead to a consistent improvement of inhomogeneous nuclear-matter properties.

9 Summary and conclusions

In this work we have extended a recent chiral approach to nuclear matter by including the effects from the most general (momentum-independent) NN-contact interaction. By iterating the combination of one-pion exchange and this two-parameter contact vertex to second order the emerging energy per particle exhausts all terms possible up to and including fourth order in the small momentum expansion. Two cut-offs $\Lambda_{0,1}$, depending on the total NN-isospin $I = 0, 1$, are introduced to regularize the (primitive) linear divergences $\int_0^\infty \mathrm{d}l\, 1$ of some three-loop in-medium diagrams. Effectively, the cut-offs $\Lambda_{0,1}$ parameterize the strength of a term linear in density, see eqs. (2), (5). The equation of state of pure neutron matter, $\bar{E}_n(k_n)$, can be reproduced very well up to quite high neutron densities of $\rho_n = 0.5\,\mathrm{fm}^{-3}$ by adjusting the strength γ_1 of a repulsive nn-contact interaction. With $\gamma_1 = -0.75$ it is comparably strong as the 1π-exchange.

Binding and saturation of isospin-symmetric nuclear matter is a generic feature of the present perturbative calculation. Fixing the maximum binding energy per particle to $-\bar{E}(k_{f0}) = 15.3\,\mathrm{MeV}$ we find that any possible equilibrium density ρ_0 lies below $\rho_0^{\max} = 0.191\,\mathrm{fm}^{-3}$. The constraint $\gamma_1 = -0.75$ from the neutron matter equation of state leads, however, to a somewhat too low saturation density of $\rho_0 = 0.134\,\mathrm{fm}^{-3}$. Fixing, on the other hand, the saturation density to $\rho_0 = 0.158\,\mathrm{fm}^{-3}$ [22] we find that the maximum binding energy per particle $-\bar{E}(k_{f0})$ lies above $10.7\,\mathrm{MeV}$.

We have also investigated the effects of the NN-contact interaction on the complex single-particle potential $U(p,k_f) + i\,W(p,k_f)$. We have found that the effective nucleon mass at the Fermi surface is bounded from below by $M^*(k_{f0}) \geq 1.4M$. The minimal effective nucleon mass occurs simultaneously together with the maximal saturation density. The corresponding parameter set $\gamma_0 = \gamma_1 = 0.39$ describes the situation in which the explicitly introduced short-range NN-terms cancel almost exactly the contact pieces of 1π-exchange. The parameter set constrained by the neutron matter equation of state leads to unrealistic real and imaginary single-particle potentials, $U(p,k_{f0})$ and $W(p,k_{f0})$, as in the scheme of Lutz *et al.* [7,10]. The downward bending of the asymmetry energy $A(k_f)$ above nuclear-matter saturation density is a generic feature of our perturbative (fourth-order) calculation. The value of the asymmetry energy at saturation density $A(k_{f0})$ is rather stable and comes out close to its empirical value $A(k_{f0}) \simeq 33\,\mathrm{MeV}$.

The properties of nuclear matter at finite temperatures have also been investigated. The critical temperature of the liquid-gas phase transition has a minimal value of $T_\mathrm{c} \simeq 21\,\mathrm{MeV}$. Good single-particle properties around the Fermi surface are a necessary condition for a realistic behavior of isospin-symmetric nuclear matter at finite temperatures $T < 40\,\mathrm{MeV}$.

The influence of the NN-contact interaction on the effective nucleon mass $\widetilde{M}^*(\rho)$ and the strength function $F_\nabla(k_f)$ of the $(\vec{\nabla}\rho)^2$-term in the nuclear energy density functional $\mathcal{E}[\rho,\tau]$ have also been studied. For the parameter set with reduced $\widetilde{M}^*(\rho)$ the prediction for $F_\nabla(k_f)$ is moved further away from the empirical band. On the other hand, the parameter set with unrealistic $\widetilde{M}^*(\rho)$ substantially improves $F_\nabla(k_f)$.

Altogether, there is within this complete fourth-order calculation no "magic" set of short-range parameters with which one could reproduce simultaneously and accurately all semi-empirical properties of nuclear matter. The conditions for a good neutron matter equation of state and for good single-particle properties (and consequently a realistic finite-temperature behavior) are in fact mutually exclusive. This clearly points at inherent limitations of the perturbative chiral approach truncated at fourth order in the small momentum expansion. While complete calculations at fifth order or even sixth order are rather demanding (four-loop and five-loop diagrams need to be

evaluated), one might also combine the chiral approach (to nuclear matter) with non-perturbative methods, as it is done commonly for free NN-scattering [20,21].

This work was supported in part by BMBF, GSI and DFG.

Appendix A.

In this appendix we take the opportunity to write down closed-form analytical expressions for the three-body and four-body contributions $W_{3,4}(p,k_f)$ to the imaginary single-particle potential as they arise from the iterated 1π-exchange Hartree diagram. Solving the integrals in eq. (22) of ref. [9] gives for the three-body term

$$\begin{aligned} W_3(p,k_f) = \frac{g_A^4 M m_\pi^4}{(8\pi)^3 f_\pi^4}\Big\{ & 35 + 151u^2 + 25u^4 - \frac{197x^2}{3} \\ & -2u^2x^2 - 7x^4 + 18\ln(1+4x^2) + \left(\frac{21}{2x} - 30x\right) \\ & \times \arctan 2x + \Big[\arctan(u+x) - \arctan(u-x)\Big] \\ & \times \frac{1}{2x}\Big[(x^2-u^2)^3 + 9(4u^2+15)(x^2-u^2) - 56\Big] \\ & +4\Big(3x^2 - 9 - \frac{2u^3}{x} - 9u^2\Big)\ln[1+(u+x)^2] \\ & +4\Big(3x^2 - 9 + \frac{2u^3}{x} - 9u^2\Big)\ln[1+(u-x)^2]\Big\}\,, \end{aligned} \tag{A.1}$$

with $x = p/m_\pi$ and $u = k_f/m_\pi$. After complete evaluation of its integral representation given in eq. (24) of ref. [9] the four-body Hartree term reads

$$\begin{aligned} W_4(p,k_f) = \frac{g_A^4 M m_\pi^4}{(8\pi)^3 f_\pi^4}\Big\{ & \frac{63x^4}{5} - 13u^4 - 7 - 2u^2(49+3x^2) \\ & + \frac{142x^2}{3} - 36\ln(1+4x^2) + \left(60x - \frac{21}{x}\right)\arctan 2x \\ & + \Big[\arctan(u+x) - \arctan(u-x)\Big] \\ & \times \frac{1}{2x}\Big[(u^2-x^2)^3 - 9x^4 - 18u^2x^2 + 27u^4 \\ & -135x^2 + 75u^2 + 49\Big] + 4(9 + 6u^2 - 2x^2) \\ & \times \ln\Big([1+(u+x)^2][1+(u-x)^2]\Big)\Big\}\,. \end{aligned} \tag{A.2}$$

Combining these novel results with the two-body Hartree term $W_2(p,k_f)$ written in eq. (20) of ref. [9] one immediately verifies Luttinger theorem [30]:

$$W_2(k_f,k_f) + W_3(k_f,k_f) + W_4(k_f,k_f) = 0\,, \tag{A.3}$$

and the zero sum-rule [9]:

$$\frac{3}{k_f^3}\int_0^{k_f} \mathrm{d}p\, p^2 \left[\frac{1}{2}W_2(p,k_f) + \frac{1}{3}W_3(p,k_f) + \frac{1}{4}W_4(p,k_f)\right] = 0\,. \tag{A.4}$$

The latter statement expresses the fact that the energy per particle $\bar{E}(k_f)$ can be reconstructed from the two-, three- and four-body contributions to the single-particle potential (graphically this is done by closing the open nucleon line of self-energy diagrams) and that no imaginary part is left over from this procedure.

References

1. A. Akmal, V.R. Pandharipande, D.G. Ravenhall, Phys. Rev. C **58**, 1804 (1998) and references therein.
2. P. Ring, Prog. Part. Nucl. Phys. **37**, 193 (1996) and references therein.
3. B.D. Serot, J.D. Walecka, Int. J. Mod. Phys. E **6**, 515 (1997) and references therein.
4. S. Typel, H.H. Wolter, Nucl. Phys. A **656**, 331 (1999) and references therein.
5. F. Hofmann, C.M. Keil, H. Lenske, Phys. Rev. C **64**, 034314 (2001) and references therein.
6. R. Brockmann, R. Machleidt, Phys. Rev. C **42**, 1965 (1990) and references therein.
7. M. Lutz, B. Friman, Ch. Appel, Phys. Lett. B **474**, 7 (2000).
8. N. Kaiser, S. Fritsch, W. Weise, Nucl. Phys. A **697**, 255 (2002).
9. N. Kaiser, S. Fritsch, W. Weise, Nucl. Phys. A **700**, 343 (2002).
10. S. Fritsch, N. Kaiser, Eur. Phys. J. A **17**, 11 (2003).
11. A. Bohr, B.R. Mottelson, *Nuclear Structure*, Vol. **I** (Benjamin, 1969) Chapt. 2.4.
12. P.E. Hodgson, *Growth Points in Nuclear Physics*, Vol. **3** (Pergamon Press, 1981) Chapt. 2.
13. S. Fritsch, N. Kaiser, W. Weise, Phys. Lett. B **545**, 73 (2002).
14. M.M. Pavan *et al.*, Phys. Scr. **T87**, 65 (2000).
15. B. Friedman, V.R. Pandharipande, Nucl. Phys. A **361**, 502 (1981).
16. R.B. Wiringa, V. Fiks, A. Fabrocini, Phys. Rev. C **38**, 1010 (1988).
17. J. Carlson, J. Morales, V.R. Pandharipande, D.G. Ravenhall, Phys. Rev. C **68**, 025802 (2003).
18. P.A. Seeger, W.M. Howard, Nucl. Phys. A **238**, 491 (1975).
19. J.P. Blaizot, Phys. Rep. **64**, 171 (1980).
20. E. Epelbaum, W. Glöckle, Ulf-G. Meißner, Nucl. Phys. A **671**, 295 (2000).
21. D.R. Entem, R. Machleidt, Phys. Lett. B **524**, 93 (2002); Phys. Rev. C **66**, 014002 (2002).
22. I. Sick, private communication. See also: D.B. Day *et al.*, Phys. Rev. C **40**, 1011 (1989).
23. D. Vretenar, G.A. Lalazissis, R. Behnsch, W. Pöschl, P. Ring, Nucl. Phys. A **621**, 853 (1997).
24. C. Mahaux, R. Sartor, Adv. Nucl. Phys. **20**, 1 (1991).
25. V.M. Galitskii, Sov. Phys. JEPT **7**, 104 (1958).
26. A.L. Fetter, J.D. Walecka, *Quantum Theory of Many-Particle Systems* (McGraw-Hill Inc., 1971) p. 148.
27. P. Grange, J.P. Cugnon, A. Lejeune, Nucl. Phys. A **473**, 365 (1987).
28. N.M. Hugenholtz, L. Van Hove, Physica **24**, 363 (1958).
29. R.W. Hasse, P. Schuck, Nucl. Phys. A **445**, 205 (1985).
30. J.M. Luttinger, Phys. Rev. **121**, 942 (1961).
31. W. Zuo, I. Bombaci, U. Lombardo, Phys. Rev. C **60**, 024605 (1999).

32. D.J. Thouless, *The Quantum Mechanics of Many-Body-Systems* (Academic Press, New York and London, 1961) Chapt. 7.3.
33. W. Kohn, J.M. Luttinger, Phys. Rev. **118**, 41 (1960); J.M. Luttinger, J.C. Ward, Phys. Rev. **118**, 1417 (1960).
34. V.A. Karnaukhov *et al.*, Phys. Rev. C **67**, 011601(R) (2003).
35. G. Sauer, H. Chandra, U. Mosel, Nucl. Phys. A **264**, 221 (1976).
36. J.I. Kapusta, *Finite-temperature Field Theory* (Cambridge University Press, 1989) Chapt. 10.
37. M. Bender, P.-H. Heenen, P.-G. Reinhard, Rev. Mod. Phys. **75**, 121 (2003) and references therein.
38. M. Beiner, H. Flocard, N. Van Giai, P. Quentin, Nucl. Phys. A **238**, 29 (1975).
39. E. Chabanat, P. Bonche, P. Haensel, J. Meyer, R. Schaeffer, Nucl. Phys. A **627**, 710 (1997); **635**, 231 (1998) and references therein.
40. J.M. Pearson, S. Goriely, M. Samyn, Eur. Phys. J. A **15**, 13 (2002); F. Tondour, S. Goriely, J.M. Pearson, M. Onsi, Phys. Rev. C **62**, 024308 (2000).
41. N. Kaiser, S. Fritsch, W. Weise, Nucl. Phys. A **724**, 47 (2003).
42. J.W. Negele, D. Vautherin, Phys. Rev. C **5**, 1472 (1972).